INL/RPT-22-66992

SPHERE Gap Conductance Test

September 2022

Zachary Sellers, Minseop Song, Jeremy Hartvigsen, and Piyush Sabharwall

MRP Microreactor Program

Idaho National Laboratory

INL is a U.S. Department of Energy National Laboratory operated by Battelle Energy Alliance, LLC

INL/RPT-22-66992

SPHERE Gap Conductance Test

Zachary Sellers, Minseop Song, Jeremy Hartvigsen, and Piyush Sabharwall

September 2022

Microreactor Program
Idaho National Laboratory
Idaho Falls, Idaho 83415

http://www.inl.gov

Prepared for the
U.S. Department of Energy
Office of Nuclear Energy
Under DOE Idaho Operations Office
Contract DE-AC07-05ID14517

Page intentionally left blank

Acknowledgments

This work was supported by the U.S. Department of Energy–Office of Nuclear Energy (DOE-NE) under the Idaho National Laboratory (INL) Advanced Reactor Technology (ART) portfolio's Microreactor Program. The authors would like to thank U.S. Nuclear Regulatory Commission (NRC) for providing feedback on this effort, namely Steve Bajorek, Tarek Zaki, and Joseph Kelly. The authors would like to thank them for their candor and support.

Page intentionally left blank

ABSTRACT

The objective of the single primary heat extraction and removal emulator (SPHERE) gap conductance test is to obtain data on the heat losses through the annular gap formed by the outer wall of the heat pipe and the inner diameter of a stainless steel core block through radiative and conductive heat transfer with varying gas compositions. This is a feature of interest for the use of heat pipes as a mechanism of heat removal from the core of an advanced nuclear reactor. The use of molten alkali metal heat pipes is being explored as part of new reactor designs. The validation of software codes and experimental support for those codes is helpful in evaluating the design of the new reactors. The heat pipe was tested at a range of powers between 300 W and 500 W. The gas compositions were atmospheric pressure nitrogen, helium, argon, and low-pressure nitrogen at 0.05 pounds per square inch absolute (psia). The gas composition changes show the change in ratio between conductive and radiative heat transfer and the trend towards the limiting case of vacuum with radiation-only heat transfer.

The results of the experimental testing of the effective heat transfer across the gap agree with the theoretical calculations. The thermal power delivered by the heat pipe to the condenser is correlated within the experimental error to the rate of heat transfer between the heater block and the heat pipe. The thermal conductivity across the gap as a function of gas composition and temperature also correlates with the expected theory. This correlates the concept of a limiting case of a heat pipe accident that the overall heat transfer across the gap aligns with the theoretical calculations.

Page intentionally left blank

CONTENTS

ABSTRACT v
ACRONYMS ix
1. INTRODUCTION 1
2. EXPERIMENTAL SETUP 2
3. TEST PROCEDURE 8
4. HEAT BALANCE ANALYSIS 9
5. RESULTS 16
6. CONCLUSION 17
7. FUTURE WORK 18
8. REFERENCES 19

FIGURES

Figure 1. SPHERE test bed with added heat tracer and insulation. 2
Figure 2. Heat pipe centerline thermocouple measurement points. 2
Figure 3. Drawing of hex block with notches. 3
Figure 4. Hex block slot locations. 3
Figure 5. SPHERE test bed wrapped in aramid insulation. 5
Figure 6. Gas gap calorimeter schematic. 6
Figure 7. Axial view of the calorimeter coupled to the heat pipe. 6
Figure 8. Long (infinite) concentric cylinders. 9
Figure 9. Boundary condition of conduction model at hex block and a sample result. 10
Figure 10. The relation between the temperature at the gap and the heat flux at different power levels. 11
Figure 11. Vacuum case – power change. 12
Figure 12. Vacuum case – temperature change at thermocouples in the thermowell. 12
Figure 13. Vacuum case – temperature change at point D. 13
Figure 14. Vacuum case – temperature at point C5. 13

TABLES

Table 1. List of required instrumentation for testing. 6
Table 2. SPHERE gap conductance test plan. 7
Table 3. Heat flux calculation for varying power levels under vacuum. 10
Table 4. Heat transfer rate for vacuum cases. 14
Table 5. Heat transfer rate for helium cases. 14
Table 6. Heat transfer rate for nitrogen cases. 15
Table 7. Heat transfer rate for argon cases. 15

ACRONYMS

ACT	Advanced Cooling Technologies
ART	Advanced Reactor Technology
CFD	computational fluid dynamics
DOE	U.S. Department of Energy
EDM	electrical discharge machining
INL	Idaho National Laboratory
J/kgK	joules per kilogram
K	Kelvin
kW	kilowatt
SCR	silicon-controlled-rectifier
SCXI	signal conditioning extensions for instrumentation
SPHERE	single primary heat extraction and removal emulator
SS	stainless steel
U.S.	United States
W	watt
W/mk	watts per meter Kelvin
W/m2k	watts per meter square Kelvin

Page intentionally left blank

SPHERE Gap Conductance Test

1. INTRODUCTION

The United States (U.S.) Department of Energy's (DOE's) Advanced Reactor Technology (ART) Microreactor Program has designed and developed the single primary heat extraction and removal emulator (SPHERE) facility and capability at Idaho National Laboratory (INL) to support non-nuclear thermal and integrated systems testing to gain a better understanding of thermal performance of heat pipes under a wide range of heating values and operating temperatures, further enhancing understanding of heat pipe startup and transient operation [1]. For the gap conductance test, a calorimeter—as well as fiberoptic, ultrasonic, and thermocouple sensors—were utilized to obtain data on the thermal conductance of the annular gap formed between a heat pipe and core block while the system was filled with varying gas compositions. The objective of the SPHERE gap conductance test was to obtain data on the heat losses through the annular gap (e.g., 0.025-in. radially) formed by the outer wall of the heat pipe and the inner diameter of a stainless steel (SS) core block through radiative and conductive heat transfer with varying gas compositions [2].

The data on the thermal conductivity of the gap allows for the total heat transfer through the gap to be obtained. This showcases how much heat loss SPHERE is losing through the core block. This allows for an understanding of the amount of heat that the heat pipe is transferring versus the amount of heat being lost through radiation and conduction through the core block.

The data from this experiment also provides insight for a larger microreactor core design. In this larger setup, the SPHERE core block will be a subsection of up to thousands of heat pipes, depending on the size of the microreactor. It is essential to understand the heat transfer of this subsection to apply the data obtained to the microreactor core design.

2. EXPERIMENTAL SETUP

The SPHERE facility consists of multiple 12-in. diameter SS sanitary tubes to allow for coupling with a wide variety of experiments. For the gap conductance test, a core block inside the tubing was wrapped with insulation and a layer of heat trace. Inside the core block, the cartridge heaters were used to heat the test article. In this case, the test article was a sodium-filled heat pipe. The heat pipe ran the entire length of the sanitary tube setup. The heat pipe had wrapped insulation and heat trace around it. The end of the heat pipe was coupled with a gas gap calorimeter for heat removal. A schematic of the gap conductance test is shown in Figure 1.

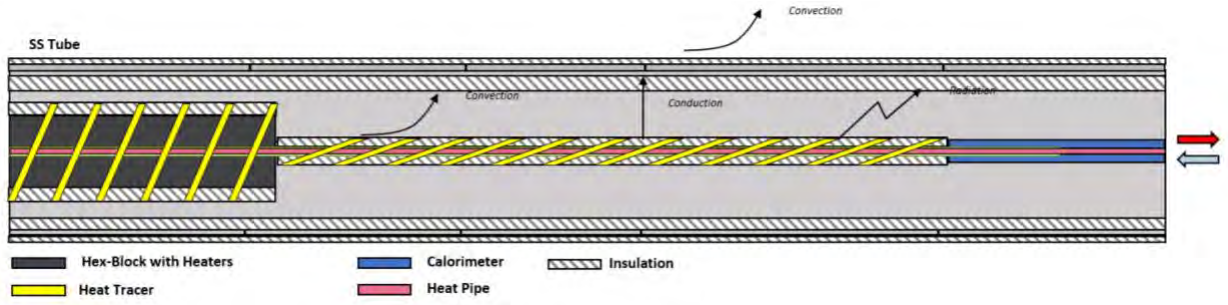

Figure 1. SPHERE test bed with added heat tracer and insulation.

The test article was a heat pipe supplied by Advanced Cooling Technologies (ACT), which was rated to an upper power limit of 1 kilowatt (kW) and used sodium as the working fluid. The heat pipe had an outer diameter of 0.625-in., while the wall thickness of the outer region measured 0.028-in. The center of the heat pipe consisted of an annular wick structure and a center region for the vapor to flow through. The wick was a 304SS screen mesh with size No.40 (0.0165-in.), which had a thickness of 0.05236-in. (e.g., 0.133 cm.) and a surface porosity of 0.686 (0.769 volumetric wick porosity). The thermal conductivity of the wick at 700°C was 35 (W/mK), which encompassed the screen and liquid sodium combined. The heat pipe had a centerline thermowell for the vapor region. The thermowell outer diameter measured 0.165-in., while the inner diameter measured 0.135-in. A multipoint thermocouple was inserted into the thermowell. The distances to the measurement points of the thermocouple are shown in Figure 2.

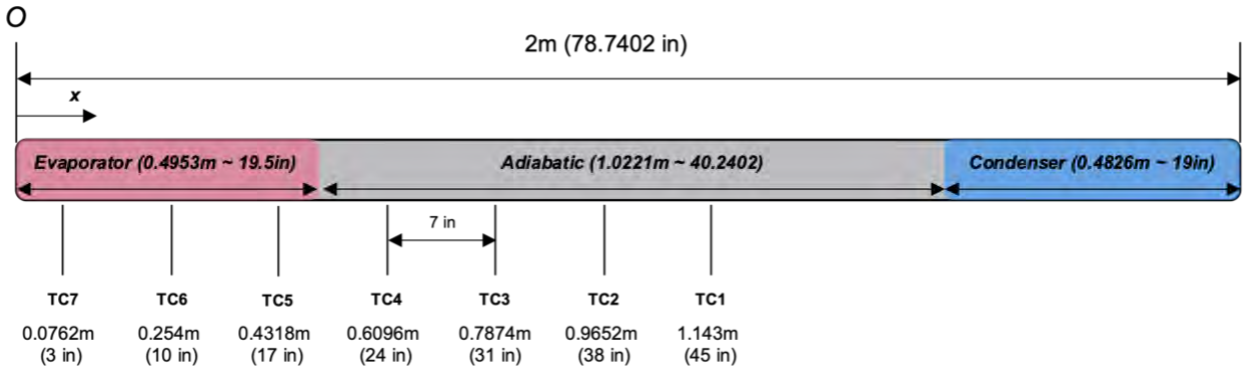

Figure 2. Heat pipe centerline thermocouple measurement points.

The core block for this experiment was a hex block made from 316SS. The total length of the hex block was 19.5-in. The core block is shown in Figure 3. The heat pipe was inserted into the hex block that was designed to simulate a subsection of common microreactor designs. A manufacturing technique known as gun drilling was utilized to drill the holes for the heaters and the heat pipe while maintaining straightness and required tolerances. Six of the holes (0.555-in.) were drilled in a circular pattern around a center hole (0.665-in.). Figure 4 illustrates the hole configuration. The hex block was then machined

using wire electrical discharge machining (EDM) to notch out sections of the heater holes as well as the center hole. These notches were used as instrumentation slots. The slots were filled with multipoint, type K thermocouples, fiberoptic temperature sensors, and an ultrasonic temperature sensor. These sensors were utilized in collaboration with INL's instrumentation team to help achieve deployment validation of these advanced sensors. The sensors also provided additional data to account for any failures with the installed thermocouples. The locations of the sensors are shown in Figure 4. Slots A, B, C, D, and E were used for the multipoint thermocouples. The remaining three slots were used for the two fiberoptic sensors and an ultrasonic sensor, respectively.

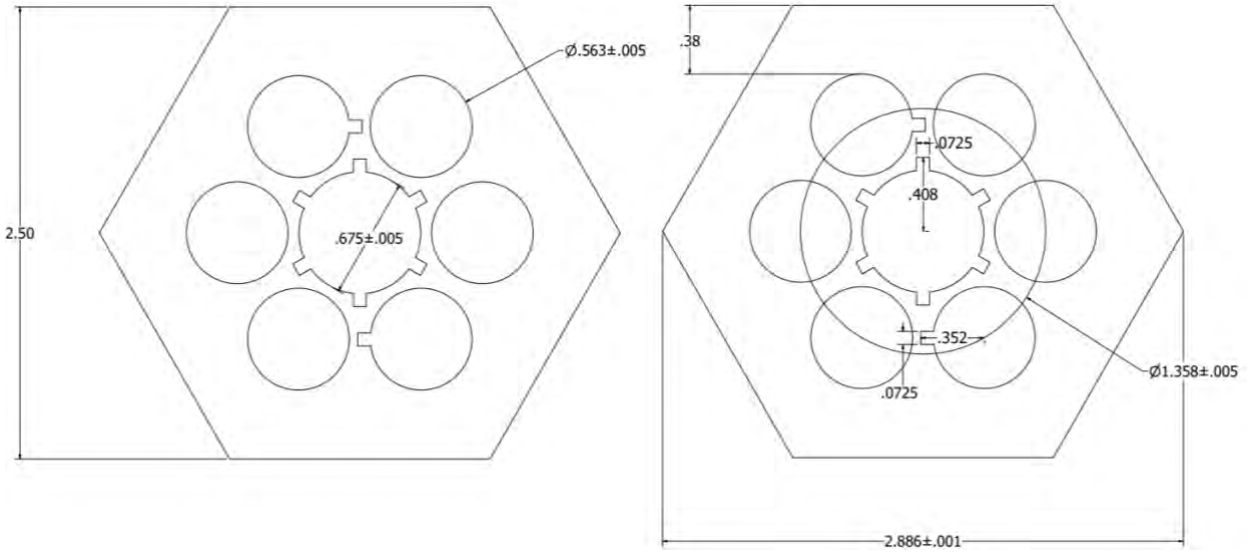

Figure 3. Drawing of hex block with notches.

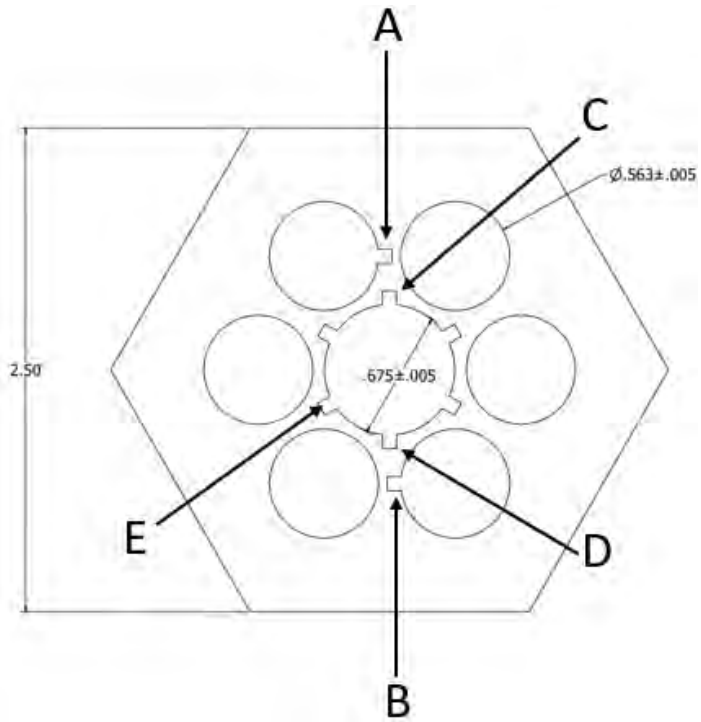

Figure 4. Hex block slot locations.

The multipoint thermocouples were procured from Idaho Labs. They had a total of 5 points. The first point was located at the front end of the core block towards the adiabatic region of the heat pipe. The other four points were spaced every 3-in.

The fiberoptic sensors ran down the axial length of the heat pipe that is located in the center hole of the hex block. Both of the sensors were able to record data down the entire length of the hex block for a total measured length of 19.5-in. to provide information for axial temperature distribution. There were two types of fiberoptic sensors used for this experiment. The first had 9 points distributed equally throughout the fiber, while the other had a spatial resolution of a data point every 6 mm (0.236-in.). Both sensors were used to record the temperature of the system.

The ultrasonic sensor also ran down the entire length of the hex block coaxial to the heat pipe. The ultrasonic sensor was able to record a sweep of data at 10 Hz, one hundred times for each steady state condition that was reached during the experiment. This allowed for the data that was collected with the ultrasonic sensor to be concise as the steady state data was the only area of interest for this experiment.

The system was coupled with a gas gap calorimeter utilizing water as the method of heat removal on the condenser end of the heat pipe. The calorimeter was centered around the heat pipe using Kanthal wire to equally space the inner wall of the calorimeter and the outer wall of the heat pipe. The wire was welded onto the outer wall of the heat pipe using a Sunstone dual pulse CD spot welder. This was done using a lower power output to confirm that the heat pipe wall was not damaged during welding. The calorimeter was connected to a ThermoFisher chiller to cool the water and form a closed loop system. The change in temperature from the inlet to the outlet was measured with a differential temperature transducer. The flow rate of this closed loop system was measured with an Adalet flow meter. These sensors worked together to collect data on the amount of heat being removed by the water at the condenser end of the heat pipe. For this experiment, a quick test was conducted to determine the accuracy of the calorimeter setup. A cartridge heater was inserted into the calorimeter and the power input was measured using a watt (W) transducer. The power out was measured using the metrics described above. Approximately 85% of the power input was transferred to the water in the closed loop of the calorimeter setup.

The experiment was heated using six 1000 W Protherm Inc. cartridge heaters. The total length for each heater was 19.5-in. with an unheated length of 0.29-in. Heater power control was achieved using Watlow Din-A-Mites silicon-controlled-rectifier (SCR)-based power controllers, which are based on a 4–20 mA control signal provided from the National Instruments signal conditioning extensions for instrumentation (SCXI) data acquisition system. This system was interfaced to a LabVIEW virtual instrument for data acquisition and instrument control. The pressure inside the heat pipes was sub-atmospheric even at the highest operating temperature, so that any failure of the heat pipe would not involve a pressurized release of material. Power to each heater was monitored continuously using precision power meters designed for measurement of SCR-controlled loads [3, 4].

The hex block was surrounded by a 1-in.-thick zirconia wool blanket using Zircar refractory insulation. The zirconia wool blanket had a thermal conductivity of 0.315 W/mk and a specific heat value of 1246 joules per kilogram (J/kgK). The adiabatic length of the heat pipe was also coated in the same style of insulation. The inner wall of the sanitary tubing was also wrapped with the 1-in.-thick zirconia wool. The final insulation layer was installed on the outer wall of the sanitary tubing. This final layer was built using an 1/8-in.-thick layer of aramid insulation. The aramid insulation had a thermal conductivity value of 0.13 W/mK and a specific heat value of 1200 J/kgK. All the zirconia wool insulation used in the system was pre-fired in an oxidizing atmosphere to remove any polymer binder. This was not done to the aramid insulation as this insulation would see max temperatures of 150°C, respectively. Both the hex block and the adiabatic section of the heat pipe were surrounded by a layer of HTS/Amptek heat trace on the outside wall of the zirconia insulation. This was done to further limit the heat losses from the outside wall of the hex block and the adiabatic region of the heat pipe. This technique is also better aligned with a realistic microreactor design. In practice, this subsection would be surrounded by more SS hex block and

heat pipe configurations. Because of this, the heat would only transfer axially down the heat pipe. The power control of the heat trace was achieved by utilizing a similar system that was described above for the cartridge heaters. Each heat trace was outfitted with two type K thermocouples. One thermocouple was used as an overtemperature controller, while the other was wired into Watlow PID controllers to allow for the system to be controlled at a constant temperature. Overtemperature control was obtained with the assistance of a Watlow overtemperature controller.

The system was equipped with a roughing pump to accomplish gas purging and allow the system to obtain a rough vacuum of approximately 25 torr. Since the system was not equipped with a turbo molecular pump, a high vacuum could not be obtained in the system leading to a small amount of conductive heat transfer to occur even in the vacuum case, but the roughing pump was adequate for the experiment overall. The modified SPHERE test bed experimental setup is shown in Figure 5. The characteristics illustrating the maximum capabilities of the test bed are as follows [1]:

- Vacuum (10^{-4} torr) or inert gas
- Multiple 12-in. diameter SS sanitary tubes
- Flanges for gas flow connections and instrumentation feedthrough ports
- A test bed designed for up to 20 kW electrical power to heaters
- Maximum test article temperature of 900°C
- Heat rejection through passive radiation and coupled with a water-cooled gas gap calorimeter. A schematic of the gas gap calorimeter is shown in Figure 6 and the calorimeter is shown in Figure 7.

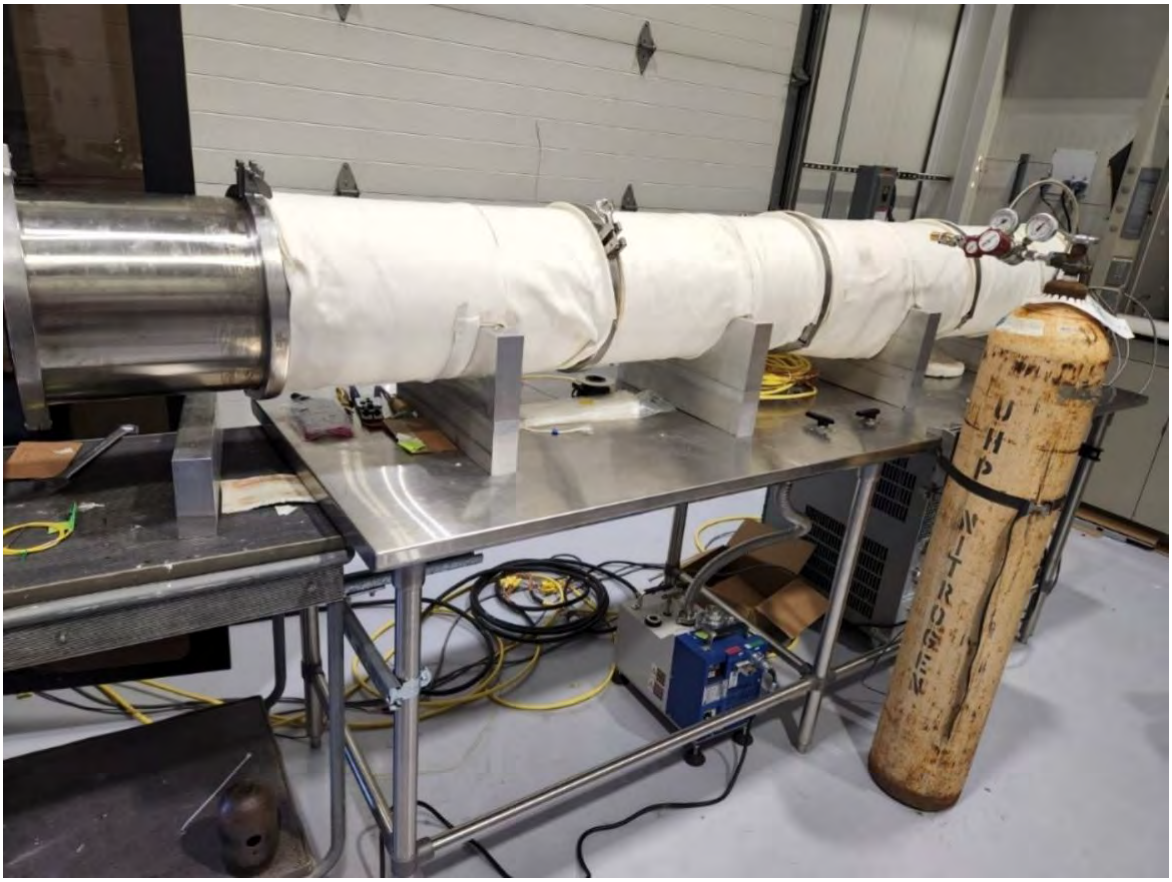

Figure 5. SPHERE test bed wrapped in aramid insulation.

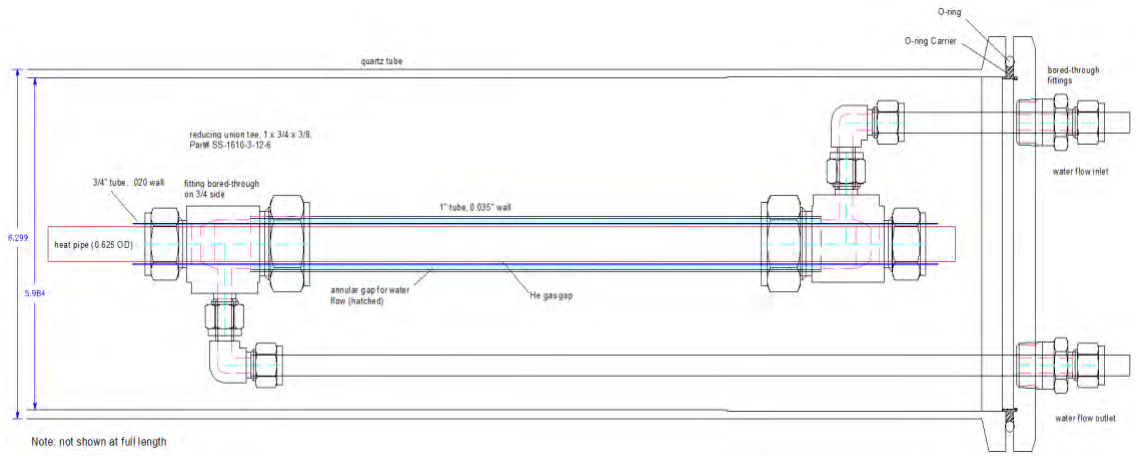

Figure 6. Gas gap calorimeter schematic.

Figure 7. Axial view of the calorimeter coupled to the heat pipe.

Instrumentation used to monitor the exterior and interior environment of the test section is shown in Table 1. These include an absolute pressure gauge, and multiple thermal sensors to help establish the full system boundary conditions for modeling purposes. Table 2 provides the gap conductance test plan with various gases and conditions, respectively.

Table 1. List of required instrumentation for testing.

Instrumentation	Quantity
Integral junction type K thermocouple	8
Multipoint type K thermocouple	6
Absolute pressure gauge	1

Table 2. SPHERE gap conductance test plan.

SPHERE Gap Conductance Test					
GAP CONDUCTANCE TEST		Condition	Measurements	Instruments	Objective
1	Pull vacuum on the tube Ramp cartridge heater power to 200W for 40 minutes Ramp heat trace temperature to create a 50C delta across boundary hold for 5 minutes Ramp Cartridge Heater Power to 500W Ramp heat trace temperature to create a 50C delta across boundary hold for length of 500W case Turn on calorimeter once centerline multipoint TC 3 exceeds 200C, run for length of experiment Hold for 8 hours while collecting steady state data Lower Power to 400W Ramp heat trace temperature to create a 50C delta across boundary hold for length of 400W case Hold for 8 hours while collecting steady state data Lower Power to 400W Ramp heat trace temperature to create a 50C delta across boundary, hold for length of 300W case Hold for 8 hours while collecting steady state data Turn off cartridge heater power Turn off heat trace power	Vacuum	Temperature, heater power Visual inspection, water cooling Fiberoptic and ultrasonic data	Type K Thermocouples Watt-Transducers Fiberoptic Sensors Distributed Multipoint Temperature Sensors Ultrasonic Sensors Delta-T Meter	Heating and control check Measure power to the cooling end as a function of temperature Measure tempearture of the annular gap Measure outside hex block temperature
2	Purge system with argon by pulling vacuum on the tube then filling with argon to 12.4 psia in a cycle five times Ramp cartridge heater power to 200W for 40 minutes Ramp heat trace temperature to create a 50C delta across boundary hold for 5 minutes Ramp Cartridge Heater Power to 500W, hold Ramp heat trace temperature to create a 50C delta across boundary hold for length of 800W case Turn on calorimeter once centerline multipoint TC 3 exceeds 200C, run for length of experiment Hold for 8 hours while collecting steady state data Lower Power to 400W Ramp heat trace temperature to create a 50C delta across boundary hold for length of 400W case Hold for 8 hours while collecting steady state data Lower Power to 300W Ramp heat trace temperature to create a 50C delta across boundary, hold for length of 300W case Hold for 8 hours while collecting steady state data Turn off cartridge heater power Turn off heat trace power	Argon	Temperature, heater power, water cooling Fiberoptic and ultrasonic data	Type K Thermocouples Watt-Transducers Fiberoptic Sensors Distributed Multipoint Temperature Sensors (Type K) Ultrasonic Sensors Delta-T Meter	Measure power to the cooling end as a function of temperature Measure tempearture of the annular gap Measure outside hex block temperature
3	Purge system with helium by pulling vacuum on the tube then filling with helium to 12.4 psia in a cycle five times Ramp cartridge heater power to 200W for 40 minutes Ramp heat trace temperature to create a 50C delta across boundary hold for 5 minutes Ramp Cartridge Heater Power to 500W, hold Ramp heat trace temperature to create a 50C delta across boundary hold for length of 500W case Turn on calorimeter once centerline multipoint TC 3 exceeds 200C, run for length of experiment Hold for 8 hours while collecting steady state data Lower Power to 400W Ramp heat trace temperature to create a 50C delta across boundary hold for length of 400W case Hold for 8 hours while collecting steady state data Lower Power to 300W Ramp heat trace temperature to create a 50C delta across boundary, hold for length of 300W case Hold for 8 hours while collecting steady state data Turn off cartridge heater power Turn off heat trace power	Helium	Temperature, heater power, water cooling Fiberoptic and ultrasonic data	Type K Thermocouples Watt-Transducers Fiberoptic Sensors Delta-T Meter Distributed Multipoint Temperature Sensors Ultrasonic Sensors	Measure power to the cooling end as a function of temperature Measure tempearture of the annular gap Measure outside hex block temperature
4	Purge system with nitrogen by pulling vacuum on the tube then filling with helium to 12.4 psia in a cycle five times Ramp cartridge heater power to 200W for 40 minutes Ramp heat trace temperature to create a 50C delta across boundary hold for 5 minutes Ramp Cartridge Heater Power to 500W, hold Ramp heat trace temperature to create a 50C delta across boundary hold for length of 500W case Turn on calorimeter once centerline multipoint TC 3 exceeds 200C, run for length of experiment Hold for 8 hours while collecting steady state data Lower Power to 400W Ramp heat trace temperature to create a 50C delta across boundary hold for length of 400W case Hold for 8 hours while collecting steady state data Lower Power to 300W Ramp heat trace temperature to create a 50C delta across boundary, hold for length of 300W case Hold for 8 hours while collecting steady state data Turn off cartridge heater power Turn off heat trace power Cool system down to room temperature	Nitrogen	Temperature, heater power, water cooling Fiberoptic and ultrasonic data	Type K Thermocouples Watt-Transducers Fiberoptic Sensors Delta-T Meter Distributed Multipoint Temperature Sensors Ultrasonic Sensors	Measure power to the cooling end as a function of temperature Measure tempearture of the annular gap Measure outside hex block temperature

3. TEST PROCEDURE

The gap conductance test was performed with a total of four gas compositions—vacuum, argon, nitrogen, and helium. The system was purged for each change in gas composition. The purging process involved pulling a rough vacuum with the test bed followed by back filling with the gas used for that portion of the experiment. This process was repeated five times for each gas to assure the system was filled with that gas exclusively. The system was then allowed to ramp up in power. The system was initially powered to 200 W and held there for 40 minutes. After this hold was complete, the heat trace was powered on to achieve a 50°C difference in temperature across the outer wall of both the heat pipe adiabatic region and the outside of the hex block. The upper testing power of 500 W was then applied to the system. Once the condenser region reached 200°C, the chiller in the calorimeter loop was powered on. Once a steady-state condition was met, the heat trace was ramped up to achieve the same 50°C difference in temperature within the same regions described above. This state was held for 8 hours to confirm steady-state. The power was then lowered to 400 W, and then down to 300 W. This procedure was followed for each of the power levels and different gas compositions. Table 2 also illustrates the experimental test plan matrix.

4. HEAT BALANCE ANALYSIS

The heat transfer within the gap includes both radiative and conductive heat transfer except in the case of a vacuum, which only includes radiation. The gap between the hex block and the heat pipe has the form of long and concentric cylinders, which enclose each other and is shown in Figure 8. This gap has a radial length of 0.025-in. In this configuration, the shape factor is equal to one, and the radiative heat flux can be calculated by Equation (2) [5]. For this equation, the two emissivity values are equal because the two materials are the same. For the case where both conductive and radiative heat transfer occur, the transfer rate can be calculated from the Equation (3) [5], which is a radial heat transfer in a cylinder geometry. The total heat transfer rate at the gap can be obtained by considering both of the heat transfer mechanisms.

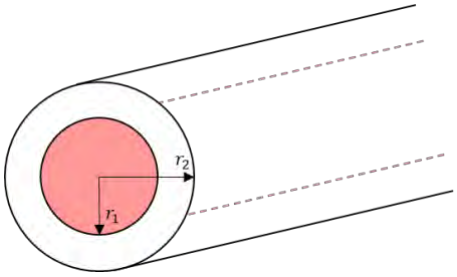

Figure 8. Long (infinite) concentric cylinders.

$$q_{12} = \frac{\sigma A_1 (T_1^4 - T_2^4)}{\frac{1}{\varepsilon_1} + \frac{1-\varepsilon_2}{\varepsilon_2}\left(\frac{r_1}{r_2}\right)} \; [W] \tag{1}$$

$$q_{12/A_1} = \frac{\sigma (T_1^4 - T_2^4)}{\frac{1}{\varepsilon_1} + \frac{1-\varepsilon_2}{\varepsilon_2}\left(\frac{r_1}{r_2}\right)} \; [W/m2] \tag{2}$$

$$q_r = \frac{2\pi L k (T_{s,1} - T_{s,2})}{\ln\left(\frac{r_2}{r_1}\right)} \; [W] \tag{3}$$

In this study, the effect of conductive heat transfer with gas was analyzed from the heat balance analysis at the gap. The gap conductance test results provide the hex block temperature at points B and D and the temperature at the thermowell, as shown in Figure 9. With the equations for the heat transfer rate for radiation and conduction, and known power delivered from hex block to heat pipe, the heat loss can be obtained.

The heat transfer rate from the hex block to the gap was calculated numerically using STAR-CCM+. When no heat loss to the outer surface of the hex block was assumed through an adiabatic condition, the maximum heat transfer rate to the gap can be obtained. The test case was made with different heater power levels varying from 300 W to 500 W, and temperatures at the boundary varying from 400°C to 800°C, respectively, as shown in Table 3 These power levels were determined by the physical limitation of the ACT heat pipe. The three-dimensional test section was constructed including a hex block, a gap, and the heaters. The hexagonal configuration of heaters is realized to reflect the geometry effect to the temperature distribution. The sample result in Figure 9 demonstrates that temperature distribution has a hexagonal shape rather than circular one. In total, 15 cases were analyzed to verify the relationship between gap temperature and heat flux with different heater power. Table 3 lists the power and T_{GAP} as a boundary condition and T_B, T_D, and the heat flux in the system, q'', as dependent variables. The heat flux at the gap increases with power, but decreases with T_{GAP}, as expected. From this data, the heat flux can be estimated from the boundary conditions. In Figure 10, the line fit to calculate heat flux from the gap temperature for each case was added. Those line fits have an R-square value higher than 0.995.

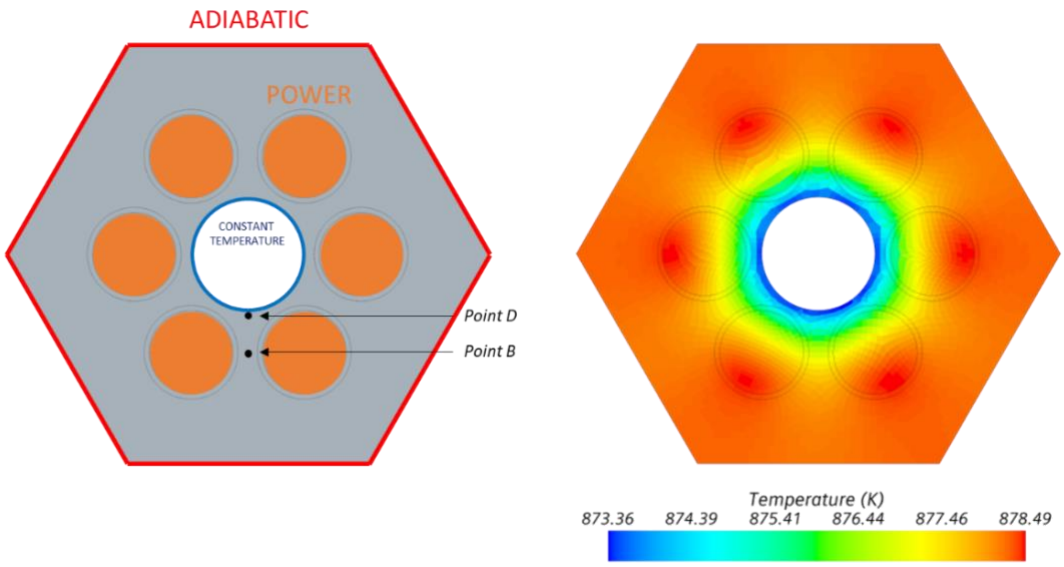

Figure 9. Boundary condition of conduction model at hex block and a sample result.

Table 3. Heat flux calculation for varying power levels under vacuum.

Power [W]	**T_{GAP} [°C]**	**T_B [°C]**	**T_D [°C]**	**$T_B - T_D$ [°C]**	**q'' [W/m^2]**
500	400	403.93	401.01	2.92	19919.2
	500	503.68	500.94	2.75	19726.7
	600	603.47	600.88	2.59	19523.2
	700	703.29	700.83	2.46	19366.5
	800	803.13	800.78	2.35	19213.1
400	400	403.14	400.81	2.34	15931.4
	500	502.95	500.75	2.20	15780.9
	600	602.78	600.70	2.07	15634.3
	700	702.63	700.66	1.97	15492.6
	800	802.50	800.62	1.88	15370
300	400	402.64	400.68	1.96	13687.1
	500	502.47	500.63	1.84	13749.8
	600	602.33	600.59	1.74	13636
	700	702.20	700.55	1.65	13524.1
	800	802.10	800.52	1.58	13412.5

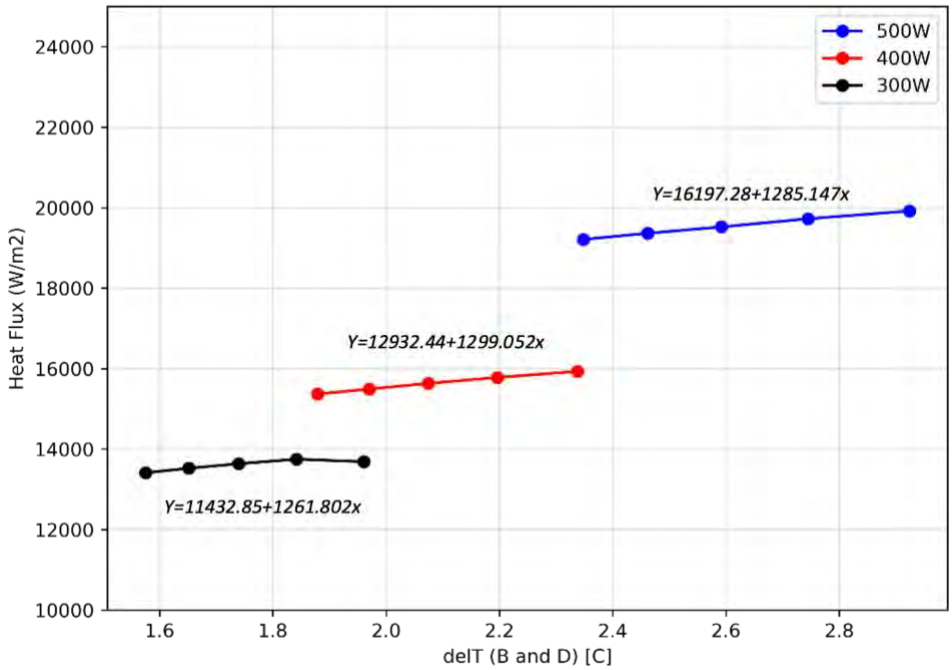

Figure 10. The relation between the temperature at the gap and the heat flux at different power levels.

The calculation of heat balance at the gap from the experimental data was made for vacuum, helium, nitrogen, and argon cases, respectively. Among them, the vacuum cases only included radiative heat transfer. Therefore, from the comparison of heat flux between the computational fluid dynamics (CFD) result and the experimental data calculation, the heat loss outside the hex block can be analyzed. Figure 11 presents the power change for the vacuum case. Power was adjusted from 500 W to 300 W. The history of temperature was depicted in Figure 12 to show the temperature at the thermowell at different power levels. The temperature at the boundary of the gap can be approximated from the temperature at point D as the temperature difference at the gap and point D is less than 1°C. The temperature at point D is higher than the heat pipe vapor as shown in Figure 13. The instrumentation experienced some oscillations, so the mean value for the temperature was taken. This was due to voltage interference from the AC heaters located closely to the thermocouple junction. The measurements from the thermocouple were validated by looking at a similarly placed thermocouple; in this case, point C, for comparison. It was found that the difference in temperature measured between the two thermocouples was within 2°C at any given point between the average temperature taken with the oscillation and the non-oscillating thermocouples. For this comparison, multipoint C5 was graphed and is shown in Figure 14.

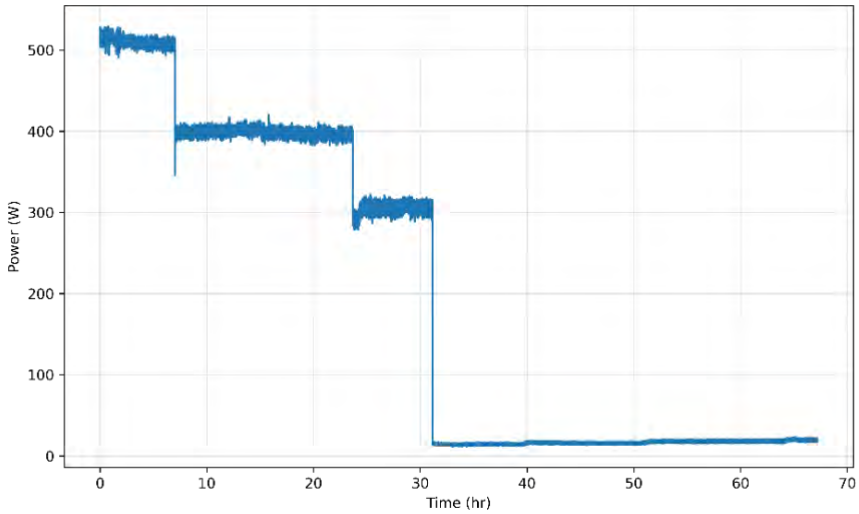

Figure 11. Vacuum case – power change.

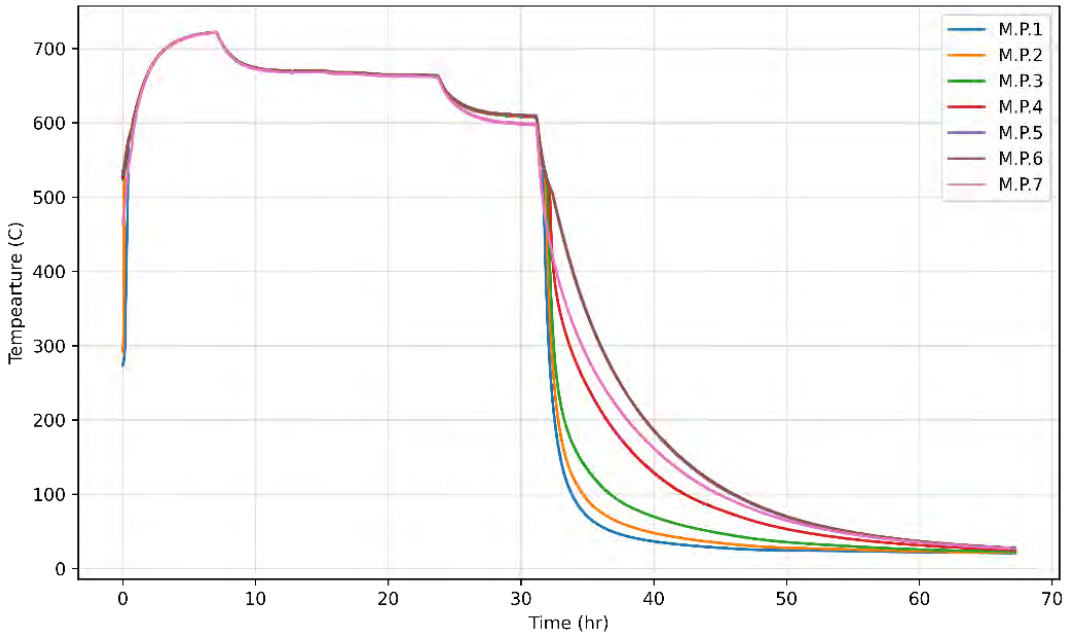

Figure 12. Vacuum case – temperature change at thermocouples in the thermowell.

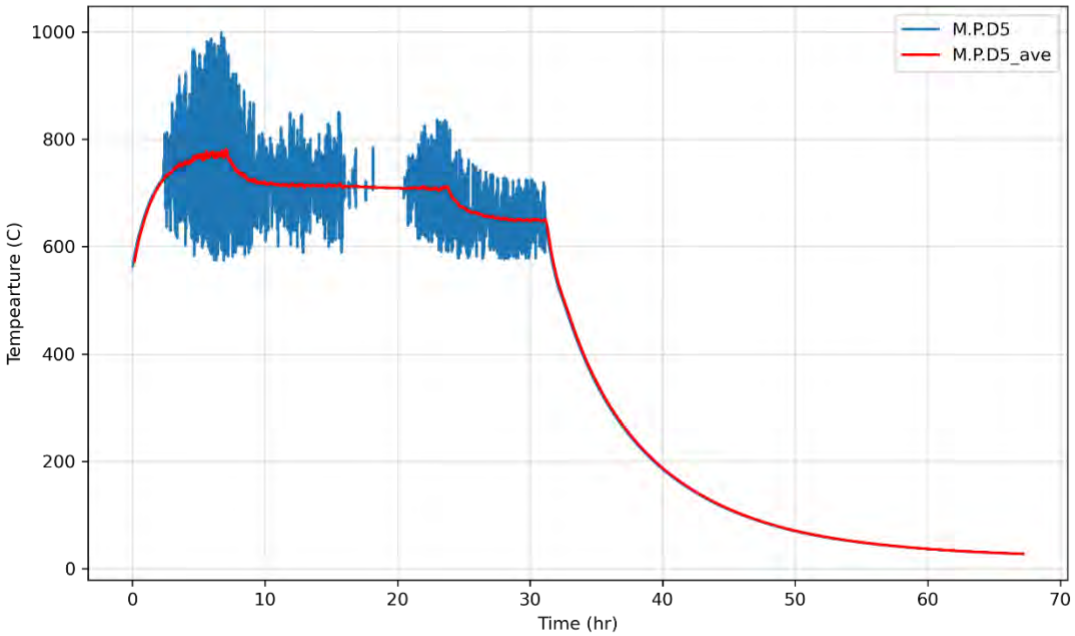

Figure 13. Vacuum case – temperature change at point D.

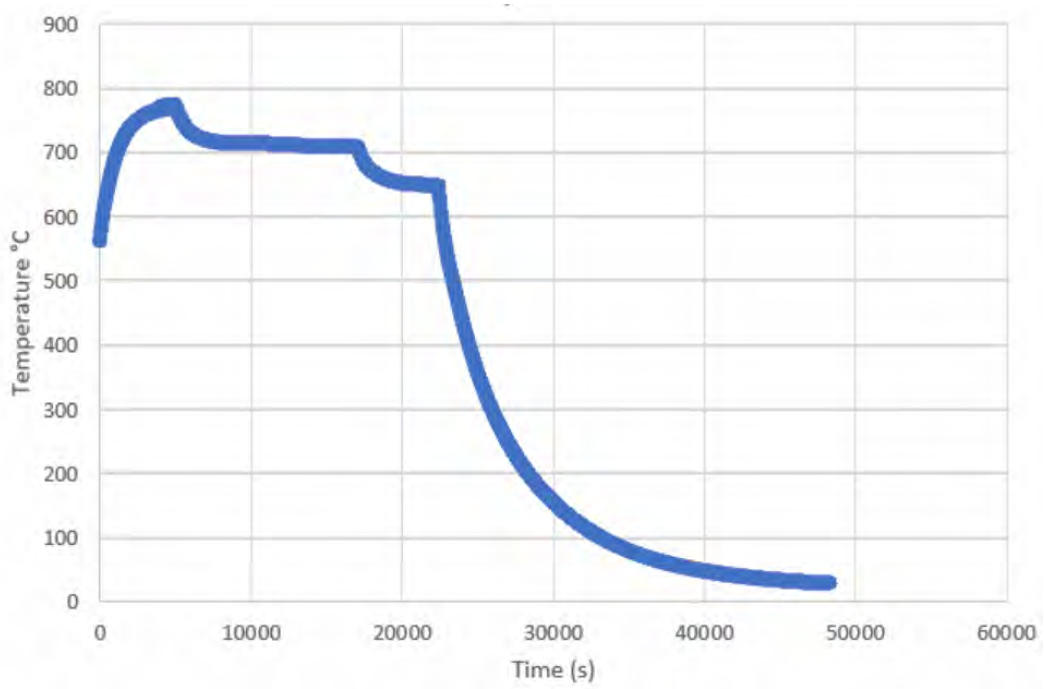

Figure 14. Vacuum case – temperature at point C5.

The heat flux comparison results for the vacuum cases is summarized in Table 4. The radiative heat flux was calculated as in q''_{rad} for the temperature data from the gap conductance test. The emissivity of SS304 of the hex block and heat pipe was assumed to be 0.73 based on the value for SS after 42 hours of heating at 527°C [6]. The maximum value of q''_{rad} was 12293 (W/m^{2}K) when the emissivity is 0.99. The radiative heat flux from the experiment is 38% of q''_{CFD}, which is the heat flux result from the CFD study at the heat pipe gap with the given temperature difference between points B and D. This is important to get an accurate heat flux with the given temperature differences. The heat transfer rate through radiative heat transfer is -176 W and conductive heat transfer at the gap is only
-3.8 W for the 500 W case. It means that there is a heat loss from the hex block to ambient in the test section. Thus, 180 W of thermal energy was transferred to the heat pipe.

For the helium, nitrogen, and argon cases where conductive heat transfer has to be considered, heat transfer was analyzed for conduction rather than radiative heat transfer. Table 5, Table 6, and Table 7 are the respective heat transfer rates for helium, nitrogen, and argon. For the helium case at 500 W, the heat transfer rate through conduction was five times higher than the radiative heat transfer. In the nitrogen and argon case, radiative heat transfer was more dominant than conduction due to the lower thermal conductivity of gas, as expected.

Table 4. Heat transfer rate for vacuum cases.

Power [W]	500	400	300
T_{GAP} (=T_D) [K]	1046.15	983.15	923.15
$T_{H.P}$ [K]	994.15	935.15	882.15
q''_{CFD} [W/m^{2}K]	-19248.00	-15480.00	-13580.60
q''_{rad} [W/m^{2}K]	-7356.49	-5643.72	-4017.53
q_{rad} [W] (ε=0.73)	-176.838	-135.666	-96.575
q_{cond} [W] (k_{air}= 0.0025 W/m-K)	-3.8839	-3.58514	-3.06231
Total q_{gap} [W]	-180.7219	-139.25114	-99.6373

Table 5. Heat transfer rate for helium cases.

Power [W]	500	400	300
T_{GAP} (=T_D) [K]	837.15	816.35	794.15
$T_{H.P}$ [K]	818.15	803.15	784.94
q_{rad} [W] (ε=0.73)	-34.4865	-22.4365	-14.5112
q_{cond} [W] (k_{helium} = 0.3 W/m-K)	-170.294	-118.31	-82.5478
Total q_{gap} [W]	-204.781	-140.746	-97.059

Table 6. Heat transfer rate for nitrogen cases.

Power [W]	500	400	300
T_{GAP} (=T_D) [K]	960.61	901.10	848.90
$T_{H.P}$ [K]	910.12	856.09	814.27
q_{rad} [W] (ε=0.73)	-132.37	-97.786	-63.774
q_{cond} [W] (k_{N2} = 0.05 W/m-K)	-75.4271	-67.2393	-51.729
Total q_{gap} [W]	-207.797	-165.025	-115.504

Table 7. Heat transfer rate for argon cases.

Power [W]	500	400	300
T_{GAP} (=T_D) [K]	1012.37	949.2236	888.03
$T_{H.P}$ [K]	961.75	901.08	840.38
q_{rad} [W] (ε=0.73)	-155.921	-122.111	-98.5104
q_{cond} [W] (k_{Argon} = 0.03 W/m-K)	-45.3664	-43.1487	-42.7021
Total q_{gap} [W]	-201.288	-165.26	-141.212

5. RESULTS

The test shows that the heat pipe operation temperature at various power levels is a significant function of the gas composition and thermal power. Table 4 showcases the total heat losses through the annular gap for the vacuum case for the varying power levels. The vacuum case was also utilized to calculate the emissivity of the system under the basis that the system would be exclusively losing heat through radiation. This emissivity value was used to calculate the radiative heat transfer for different gas compositions (e.g., helium, nitrogen, argon) in the system. The roughing pump used to pull vacuum on the system could only pull a rough vacuum of approximately 3400 Pa. This resulted in a small amount of heat transfer losses through conduction for even the vacuum case. The vacuum radiative heat losses for the 500 W, 400 W, and 300 W cases were 176.84 W, 135.67 W, and 96.58 W, respectively, while the conductive heat losses were 3.88 W, 3.59 W, and 3.06 W, respectively. These losses resulted in a total gap heat loss of 180.72 W, 139.25 W, and 99.64 W, respectively. These values closely matched the expected results for the losses through the core block.

The remaining gas compositions had a higher mixture of conductive and radiative heat transfer losses through the gap. The total amount of heat transfer was a function of the thermal conductivity of the gases as well as the varying power levels of the system. Table 5 illustrates the heat transfer losses for the helium case. The helium radiative heat losses for the 500 W, 400 W, and 300 W cases were 34.49 W, 22.44 W, and 14.51 W, respectively, while the conductive heat losses were 170.29 W, 118.31 W, and 82.55 W, respectively. These losses resulted in a total gap heat loss of 204.78 W, 140.75 W, and 97.05 W, respectively. The radiative heat transfer for the helium was significantly lower than the other cases due to the high amount of heat transfer through conduction given the higher thermal conductivity of the gas. The overall temperature of the system was approximately 150–200 degrees lower than the other gas compositions.

Table 6 highlights the heat transfer losses for the nitrogen case. The nitrogen radiative heat losses for the 500 W, 400 W, and 300 W cases were 132.37 W, 97.79 W, and 63.77 W, respectively, while the conductive heat losses were 75.43 W, 67.24 W, and 51.73 W, respectively. These losses resulted in a total gap heat loss of 207.80 W, 165.03 W, and 115.50 W, respectively. The nitrogen total heat losses were similar to the total heat losses from the helium, but the breakdown of the heat losses was different. The helium case had a larger amount of conductive heat transfer while the nitrogen had a larger amount of radiative heat transfer.

Table 7 showcases the heat transfer losses for the argon case. The argon radiative heat losses for the 500 W, 400 W, and 300 W cases were 155.92 W, 122.11 W, and 98.51 W, respectively. The conductive heat transfer losses were 45.37 W, 43.15 W, and 42.70 W, respectively. The total heat losses for the argon case were 201.29 W, 165.26 W, and 141.21 W, respectively. The conductive heat transfer for the argon case was consistent for each power case while the radiative heat losses experienced larger drop offs. The total heat losses for the argon cases closely matched the previous gas compositions. The 300 W case for argon did have a larger amount of heat transfer losses through the gap compared to the other gas compositions. These results are consistent with the expected values. The main mode of heat transfer was radiative due to the lower thermal conductivity of the gas.

The results of this work are in close alignment with predicted behavior for one-dimensional heat transfer for solid bodies. The convective phase-change heat transfer of the heat pipe itself does not significantly alter the behavior at the fuel and heat pipe wall. Future work would focus on increasing the capability by improving the guard heating units. This would include upgrading the heat trace wrapped around the adiabatic and evaporator sections of the system. These improvements would provide a higher fidelity comparison between the individual element that SPHERE represents and the larger, full-scale system of the microreactor concept. In the full-scale version, there would be hundreds to thousands of these seven-hole configurations in the core block. Because of this, the outside region of the SPHERE evaporator section should be close to adiabatic to align closer to the actual reactor core design.

6. CONCLUSION

This experiment was set up and run to accomplish the task of finding the heat losses through the annular gap that is formed between the wall of the core block and the heat pipe outer wall with varying gas compositions and power levels. The theory and experimental results agree closely. This gives confidence in using standard assumptions for modeling the heat transfer between a heat pipe and a fuel rod. The heat losses through the gap were in close agreement with what was expected. For every gas composition and power level, the power loss through the gap was consistent. The heat transfer to the heat pipe, and therefore down the axial length to the adiabatic and evaporator region, was between 20–40% of the total power input. This results in approximately 60–80% of the power input being transferred to other areas outside the heat pipe. The breakdown of the heat transfer was different for each gas composition. The vacuum case was almost entirely radiative heat transfer. The other gas compositions were a mixture of conductive and radiative heat transfer. The fraction of these two modes was a function of the thermal conductivity of the gases, respectively.

7. FUTURE WORK

To expand on the knowledge of the heat transfer throughout the system, the heat balance for the entire system should be calculated. This can be accomplished with the use of heat flux meters. Future work on this gap conductance experiment would use these heat flux meters on the outer surfaces of the hex block, as well as potentially on the outside of the adiabatic region of the heat pipe. This would allow for a more complete analysis of the heat balance throughout the entire system as the data obtained from the gap conductance experiment only shows the heat transfer through the annual gap.

8. REFERENCES

1. Idaho National Laboratory (INL), 2022, "SPHERE Factsheet," INL, Idaho Falls, ID, USA. [online]. Available at: https://gain.inl.gov/SiteAssets/MicroreactorProgram/SPHERE_Factsheet_MRP_May2022.pdf (last accessed 27 September 2022).
2. Sabharwall, P., J. Hartvigsen, T. Morton, Z. Sellers, and J. S. Yoo, 2020, *SPHERE Assembly and Operation Demonstration*, INL/EXT-20-60782, December 2020, Idaho National Laboratory, Idaho Falls, ID, USA. https://doi.org/10.2172/1824206.
3. Sellers, Z., P. Sabharwall, J. Hartvigsen, and M. Song, 2022. *SPHERE Gas Composition Test and SOCKEYE Validation*, INL/RPT-22-66992, July 2022, Idaho National Laboratory, Idaho Falls, ID, USA.
4. Hansel, J., J. Hartvigsen, L. Ibarra, P. Sabharwall, and B. Feng, 2022, "SOCKEYE Validation Support Using the SPHERE Facility," *International Conference on Physics of Reactors 2022* (*PHYSOR 2022*), Pittsburgh, PA, USA, 15–20 May 2022.
5. Incropera, F. P., and D. P. DeWitt, 1990, *Introduction to Heat Transfer*, Wiley, New York, NY, USA.
6. Grünewald, H., 1972, *Handbook of Chemistry and Physics*, Chemical Rubber Co., Cleveland, OH, USA.